

NIST Special Publication 250-97

**Magnetic Resonance Imaging
Biomarker Calibration Service:
Proton Spin Relaxation Times**

Michael A. Boss
Andrew M. Dienstfrey
Zydrunas Gimbutas
Kathryn E. Keenan
Anthony B. Kos
Jolene D. Splett
Karl F. Stupic
Stephen E. Russek

This publication is available free of charge from:
<https://doi.org/10.6028/NIST.SP.250-97>

NIST
**National Institute of
Standards and Technology**
U.S. Department of Commerce

NIST Special Publication 250-97

Magnetic Resonance Imaging Biomarker Calibration Service: Proton Spin Relaxation Times

Michael A. Boss
Kathryn E. Keenan
Karl F. Stupic
Stephen E. Russek
*Applied Physics Division
Physical Measurement Laboratory*

Andrew M. Dienstfrey
Zydrunas Gimbutas
*Applied and Computational Mathematics Division
Information Technology Laboratory*

Anthony B. Kos
*Quantum Electromagnetics Division
Physical Measurement Laboratory*

Jolene D. Splett
*Statistical Engineering Division
Information Technology Laboratory*

This publication is available free of charge from:
<https://doi.org/10.6028/NIST.SP.250-97>

May 2018



U.S. Department of Commerce
Wilbur L. Ross, Jr., Secretary

National Institute of Standards and Technology
Walter Copan, NIST Director and Undersecretary of Commerce for Standards and Technology

Certain commercial entities, equipment, or materials may be identified in this document in order to describe an experimental procedural or concept adequately. Such identification is not intended to imply recommendation or endorsement by the National Institute of Standards and Technology, nor is it intended to imply that the entities, materials, or equipment are necessarily the best available for the purpose.

National Institute of Standards and Technology Special Publication 250-97
Natl. Inst. Stand. Technol. Spec. Publ. 250-97, 35 pages (May 2018)
CODEN: NSPUE2

This publication is available free of charge from:
<https://doi.org/10.6028/NIST.SP.250-97>

Abstract

This document describes a calibration service to measure proton spin relaxation times, T_1 and T_2 , of materials used in phantoms (calibration artifacts) to verify the accuracy of magnetic resonance imaging (MRI)-based quantitative measurements. Proton spin relaxation times are used as image-based biomarkers to assess the state of tissue and quantify the presence of contrast agents. A biomarker, as defined by the U.S. Food and Drug Administration definition, refers to “a characteristic that is objectively measured and evaluated as an indicator of normal biological processes, pathogenic processes, or biological responses to a therapeutic intervention.”[1] Spin relaxation times are phenomenological parameters that must to be carefully defined and measured to enable rigorous quantification and their use as biomarkers for clinical decision making. The relaxation times, in addition to being dependent on local material properties, are dependent on environmental parameters such as temperature and magnetic field strength, which must to be controlled and precisely measured.

Key words

Biomarker; MRI; magnetic resonance imaging; T_1 ; T_2 ; NMR; nuclear magnetic resonance; proton spin relaxation times.

Table of Contents

1. Introduction	1
2. Calibration Service Summary	1
3. Theory of Measurement	2
3.1. System Basics and Measurement Principle	2
3.2. Measurement Equations	4
3.3. Model Errors	6
4. Measurement System.....	7
4.1 NMR system	8
4.2 Fiber optic temperature probe and temperature control system.....	10
5. Standard Operating Procedures.....	11
5.1 System Startup	11
5.3 Data Acquisition	12
5.4 Data Analysis	13
6. Uncertainty Evaluation	15
6.1. Overview of Measurement System Uncertainties	17
6.2 Non-Ideal Pulse Sequence (NPS)	19
6.3 Local Environment Variation (LE).....	20
6.4 Non-ideal Material properties (NM).....	21
7. Monte Carlo Uncertainty Calculation	22
8. Quality Control	26
9. Summary	27
References.....	28
Appendix A: Lack of Fit Test.....	29

List of Tables

Table 1. Phase cycling scheme.	12
Table 2. Results of Monte Carlo calculations of bias (mean) and standard deviation associated with T_1 , T_2 measurements.	26

List of Figures

Fig. 1. (a) Synthesized data from an inversion recovery experiment. (b) Residuals showing structure indicative that the model is not appropriate.....	7
-------------------------------------------------------------------------------------------------------------------------------------------------------	---

Fig. 2. Schematic diagram of the NIST NMR measurement system	8
Fig. 3. (a) Nutation data for a MnCl_2 solution (T2-9) at 20 °C. Red line is a fit using a model where the RF amplitude and coil sensitivity function are given by the graph in (b).	10
Fig. 4. Screen shot of sample temperature control software with the temperature monitored for 20 min.....	11
Fig. 5. Sample capillary and fiber optic thermometer inserted into NMR tube.	12
Fig. 6. Inversion recovery data for a NiCl_2 solution.....	14
Fig. 7. T_2 measurement of same sample as used in Fig. 6.	15
Fig. 8. NMR system schematic with labeled sources of uncertainty.....	18
Fig. 9. Schematic of Monte Carlo calculation.....	23
Fig. 10. T_1 and T_2 distributions from Monte Carlo calculations.....	24

1. Introduction

This calibration service provides traceable measurements of the proton spin¹ relaxation times, T_1 and T_2 , of materials used in magnetic resonance imaging (MRI) phantoms (calibration artifacts) at a specified field strength and temperature. T_1 is the longitudinal relaxation time, the exponential time constant required for the nuclear magnetization to relax back to its equilibrium value along the static magnetic field direction. T_2 is the transverse relaxation time, the exponential time constant required for the precessional component of the nuclear magnetization, transverse to the static field, to relax back to zero. Precise definitions of T_1 , T_2 are given in Sec. 3. *Here, we restrict measurements to water-proton magnetic moment relaxation in aqueous solutions.* The measurements are based on a variable-field, variable-temperature, nuclear magnetic resonance (NMR) system. NMR and MRI systems are qualitatively similar; however, given the smaller sample volumes in NMR systems, key parameters such as radio frequency (RF) field intensity, magnetic field distortions, and the timing of RF pulses can be better controlled and made more precise. Hence, NMR is a better system for primary measurements of key MRI biomarkers.

2. Calibration Service Summary

The relaxation time measurements are performed in an NMR system at clinical MRI magnetic fields of 1.5 T, 3.0 T, 7.0 T, with variable sample temperatures between 0 °C to 50 °C. The customer's aqueous solutions, or materials under test, are sent to NIST and the customer specifies the desired measurement fields and sample temperatures. The sample volume for measurement is approximately 20 μl . It is recommended that at least 5 ml be provided by the customer to ensure that several samples can be taken and to minimize effects due to evaporation or surface contamination. The dynamics of the magnetic moment of the customer's material solutions must conform with the Bloch equations with single exponential relaxation times as described in Sec. 3. The samples must be stable for the duration of the measurement process. At the completion of the calibration measurements, the material under test and a calibration report are sent to the customer. The calibration report summarizes the results of the measurements and provides a statement of the total measurement uncertainty (bottom line in Table 2). The service identification for the measurement service in this document is 80010C, 80011C.

The NMR system calibration is detailed in Secs. 4 and 5, with a short summary given here. The NMR time base is calibrated with a rubidium frequency standard that is first verified against a NIST-traceable rubidium atomic clock. The temperature is monitored using a non-magnetic fiber optic probe that is verified using NIST-traceable platinum resistance thermometers and ice-point calibrations. The main DC magnetic field, B_0 , is determined after shimming² to an accuracy of 10^{-6} (1 ppm³) by the resonant frequency of protons in water based on the Committee on Data for Science and Technology (CODATA) value of the water proton gyromagnetic ratio. The RF probe is tuned and matched before

¹The proton spin refers to both the proton angular momentum and the associated magnetic moment. The magnetic moment is observed experimentally.

² Shimming refers to homogenizing the magnetic field around the sample by adjusting the currents in a set of superconducting and room temperature shim coils. Our system has 9 superconducting and 17 room temperature shim coils.

³ The local field experienced by a water proton in a sample may differ from the B_0 field by several ppm depending on the susceptibility and configuration of sample inserted. The local field is a combination of B_0 field, applied gradient fields, magnetic fields generated by the sample and sample container, microscopic fields, and other environmental fields.

and after the shimming. The NMR RF power calibration is done before each series of measurements using nutation experiments described in Sec. 4.1. The instrument linewidth, the minimum linewidth obtainable by the system, is measured on narrow linewidth samples including a standard sample 3.0 % chloroform and 0.2 % tetramethylsilane (TMS) in deuterated acetone (DLM5000 from Cambridge Isotope Laboratories) and deionized water samples in the standard sample configuration. The instrument linewidth, after shimming, should be less than 1 Hz full-width at half-maximum (FWHM). Finally, the NMR system is reshimmmed for each material under test, and the linewidth is minimized to ensure that intrinsic line-broadening effects dominate the effects of B_0 nonuniformity on linewidth. The proton spin relaxation times are measured using standard pulse sequences, detailed in Sec. 5.3 and in standard texts such as *200 and More NMR Experiments: A Practical Course*, S. Berger & S. Braun; and *Pulse and Fourier Transform NMR; Introduction to Theory and Methods*, T. Farrar & E. Becker [2, 3].

Our relaxation time measurements, unlike many past efforts [4], include precise temperature control because most materials have a substantial temperature dependence of the relaxation times. There are tradeoffs in the ability to simultaneously minimize uncertainties in NMR-based parameters and sample temperature. The relaxation times, given that the material satisfies the model constraints detailed in Secs. 3.2, 3.3, are measured with a coefficient of variation (CoV) of less than 1 % at a particular temperature and field strength. The total relative uncertainty in the T_1 , T_2 measurements are typically $\left(0.5 + 0.15 \text{ }^\circ\text{C} \frac{100}{T_{1,2}} \frac{\partial T_{1,2}}{\partial T_s}\right) \%$, where the change in the T_1 , T_2 relaxation times with the sample temperature T_s are typically in the range of 2 % / $^\circ\text{C}$.

3. Theory of Measurement

3.1. System Basics and Measurement Principle

The proton spin relaxation of a spin packet⁴ located at position \vec{r} in an applied magnetic field B_0 along the z -axis is measured by monitoring the relaxation of the proton magnetization $\vec{M}(t) = \frac{\sum_i \langle \vec{\mu}_i \rangle}{V_s}$ where $\langle \vec{\mu}_i \rangle$ is the expectation value of the magnetic moment of the i^{th} proton in the volume V_s of the spin packet. We assume that the time evolution of the local magnetization is given by the Bloch equation [5]:

$$\frac{d\vec{M}(\vec{r}, t)}{dt} = \gamma_{wp} \vec{M} \times \vec{B} - \frac{M_z - M_0}{T_1} \hat{z} - \frac{\vec{M}_t}{T_2}, \quad (1)$$

where γ_{wp} is the water proton gyromagnetic ratio, $\vec{B} = \vec{B}_0 + \vec{B}_L + \vec{B}_1(t) + \vec{B}_n(t)$ is the magnetic flux density at the spin packet, \vec{B}_0 is the macroscopic main field due to the solenoid and shim coils, \vec{B}_L is

⁴ A spin packet, often referred to as an isochromat, refers to an ensemble of like spins, which is spatially large on the atomic scale, but very small on the scale of the variations in local magnetic fields. Spins are alike if they belong to the same species, are in the same chemical environment, and are in the same structural environment, e.g., they are all flowing together. We prefer the use of “spin packet” to isochromat, since isochromat originally referred to spins with the same Larmor frequency; we are generalizing to similar spins sharing a similar environment.

the local fields produced by the sample, $\vec{B}_1(t)$ is the applied time dependent RF fields, $\vec{B}_n(t)$ is the field created by environmental and thermal noise, T_1 is the longitudinal spin relaxation time, $\vec{M}_t = M_x\hat{x} + M_y\hat{y}$ is the transverse component of the proton magnetization, and T_2 is the transverse spin relaxation time. The equilibrium proton magnetization M_0 is

$$M_0 = \frac{\hbar^2 \gamma_{wp}^2 B_0 N_p}{4k_b T_s}, \quad (2)$$

where T_s is the sample temperature, N_p is the number of protons per unit volume, \hbar is the reduced Planck constant, and k is the Boltzmann constant. The B_0 field is assumed to be much larger than all other field components. For measurements performed under the service described here, B_0 is at least a factor of 10^4 greater than the other listed field components. In the absence of any other fields the magnetization will precess about the B_0 field at the left-handed Larmor frequency:

$$f_0 = \frac{\gamma_{wp}}{2\pi} B_0. \quad (3)$$

The proton magnetization vector can be manipulated by application of RF fields perpendicular to B_0 and alternating at the Larmor frequency, which is 63.9 MHz, 128 MHz, and 298 MHz for field values of interest (1.5 T, 3.0 T, and 7.0 T). By application of RF fields (referred to as B_1 fields), the magnetization experiences a torque causing rotation away from B_0 . The application of resonant RF pulses for specific durations will cause the magnetization to rotate and thereby acquire a component in a plane transverse to B_0 ; where it will precess about B_0 at the Larmor frequency, enabling inductive detection of the nuclear magnetization.

The Bloch equation is phenomenological and must be applied carefully. It often does not apply to spin systems with spin greater than $\frac{1}{2}$ because, in higher spin systems, there are many excitation levels which can have different relaxation time constants. The Bloch equation does not predict important effects such as spin echoes. To model spin echoes, an ensemble of spin packets, each obeying a Bloch equation with different local parameters, is required. We refer to the model using a linear superposition of a large ensemble of spin packets, with varying properties and local fields, each obeying the Bloch equation, as the *Bloch Model*. While T_1 , which is an energy relaxation time is well defined, T_2 is not [5]. Transverse spin relaxation can be due to either reversible spin dephasing, such as that caused by static spatial variation in field values \vec{B}_0, \vec{B}_L , or due to irreversible dephasing effects, which comprise the T_2 term. The spin dephasing rate, $\frac{1}{T_2^*}$, is the sum of two terms [5, 6]:

$$\frac{1}{T_2^*} = \frac{1}{T_2'} + \frac{1}{T_2}, \quad (4)$$

The first term, $\frac{1}{T_2'}$, is usually thought of as encompassing extrinsic dephasing processes; the second, $\frac{1}{T_2}$, as encompassing intrinsic dephasing processes. The distinction between the extrinsic and intrinsic dephasing processes is not unique, and an operational definition of T_2 is required. The definition of T_2 that will be used in this calibration service is described in Sec. 3.2.

There is a large literature on nuclear spin relaxation with a recent comprehensive review given in Ref. [7]. There are many different methods to measure T_1 [8], and new methods are published each year. Many of the proposed T_1 -measurement methods are focused on faster, lower power techniques that are pragmatic for use in MRI on human patients. Similarly, there is extensive literature on measuring T_2 as well as analysis of sources of error in these measurements [4]. The purpose of this report is not to compare measurement methods, but to document best practices to measure T_1 and T_2 using the most basic and proven methods and thus to allow validation of other techniques that may be more appropriate for advanced applications that require fast or low power acquisition.

3.2. Measurement Equations

T_1 Measurement Equations

The time dependence of the longitudinal proton magnetization M_z , in the presence of only the static applied field along the z-direction, can be determined from Eq. (1) and is given by:

$$M_z(t) = M_{zi} + (M_0 - M_{zi}) \left(1 - e^{-\frac{t}{T_1}} \right), \quad (5)$$

where M_{zi} is the initial component of the z-axis magnetization. For our T_1 measurements, an inversion-recovery sequence is used (see Sec. 5.3 for details), which starts by inverting the magnetization, initially along $+\hat{z}$, with a composite 180° pulse that rotates the magnetization about the x' axis or y' axis, where x' , y' are the x , y axes in the rotating frame. Usually, a set of pulse excitations are used with different phases, referred to as phase cycling, that rotate the magnetization about different axes to average out imperfections in the RF pulse amplitudes and phases. The initial time, $t = 0$, is defined as the time just after completion of the composite 180° pulse. The longitudinal magnetization is sampled at time TI when a detection 90° RF pulse is applied to tip the magnetization into the transverse plane. The free induction decay (FID) of the precessing transverse magnetization, for $t > TI$, is then recorded as a complex voltage signal across the RF receive coil, with both amplitude and phase information:

$$S(t) = S(0)e^{-i\omega_0(t-TI)} e^{-\frac{t-TI}{T_2^*}}. \quad (6)$$

Here, $S(0) \propto M_z(TI)$, which varies from negative to positive values as TI increases. While the signal is acquired at the precessional frequencies of the protons being sampled, the signal is mixed down to intermediate frequencies before digitization and then further digitally processed to get a signal at a

frequency that is the difference between the transmit frequency and the receiver local oscillator frequency. The data are then Fourier transformed, with a standard discrete fast Fourier transform technique, to obtain a Lorentzian of the form

$$S'(\omega) = \frac{S(0)T_2}{1 + T_2^2(\omega - \omega_0)^2}; S''(\omega) = \frac{S(0)T_2^2(\omega - \omega_0)}{1 + T_2^2(\omega - \omega_0)^2}, \quad (7)$$

where S' and S'' are the real and imaginary parts of the Lorentzian, respectively. The full width at half maximum (FWHM) of the Lorentzian is $\Delta\omega = 2/T_2$, or when plotted as a function of frequency, is $\Delta f = 1/\pi T_2$. The Fourier transform of the FID data will be referred to as spectral data or just spectra. The real part of the Lorentzian is integrated to give an integrated signal $S_i = \pi S(0) \propto M_z(TI)$ of the form

$$S_i(TI) = A \left(1 - Be^{-\frac{TI}{T_1}} \right). \quad (8)$$

While we use $S_i(TI)$ as a measure of $M_z(TI)$, alternative methods to obtain a value proportional to $M_z(TI)$ are available, including using the initial value of the measured FID or the integrated magnitude of the FID. The use of $S_i(TI)$ has the advantage of isolating a particular spin packet in the event that several components exist with different resonant frequencies.

Long delay times, $TD > 5T_1$, where TD is the time between the 90° readout pulse and the next 180° composite excitation pulse, are used so the magnetization recovers to within $e^{-5} \approx 0.7\%$ of its equilibrium value. For the inversion recovery sequence, the repetition time, the time between consecutive 180° composite excitation pulses, is given by $TR = TI + TD$.

T_2 Measurement Equations

T_2 is the time it takes for the transverse proton magnetization $M_t(\vec{r}, t)$ of a localized spin packet to relax back to its equilibrium value of 0 so that

$$M_t(\vec{r}, t) = M_t(0)e^{-\frac{t}{T_2}}. \quad (9)$$

The signal is, however, composed of many spin packets at different locations within the sample. Each location may have a different local field causing the observed signal to dephase faster than each individual spin packet. To remove this dephasing effect, which is often an extrinsic effect not related to the microscopic properties of the sample, a series of refocusing pulses is used. The spins are tipped

into the transverse plane using a 90° excitation pulse. A series of 180° pulses are then applied with a time interval τ_{cp} before and after the 180° pulse.⁵ The spin echo period is then $2\tau_{cp} + t_{180}$. After n refocusing pulses at a time $t_a = n(2\tau_{cp} + t_{180})$ after the completion of the 90° excitation pulse, a free induction decay is recorded. To determine a quantity proportional to the magnitude of the transverse magnetization at time t_a , the FID is Fourier transformed and the real part is integrated, as in Eq. (7) above. The integrated spectra give a collection of signals, $S(t_a)$, which have a simple exponential decay:

$$S(t_a) = S_0 e^{-\frac{t_a}{T_2}}. \quad (10)$$

The details of this Carr-Purcell-Meiboom-Gill (CPMG) sequence [9] are discussed in Sec. 5.3, and typical data are presented in Sec. 5.4.2. While we use a multi-refocusing sequence here for primary NMR measurements, it may not be suitable for primary MRI measurements since complications in MRI, which include slice select, band limited pulses, larger B_0 inhomogeneity and dispersion in tipping angles may make these multi-refocusing less accurate than sequences with a single refocusing pulse.

Other methods exist for obtaining a quantity proportional to the transverse magnetization, including integrating the real part of the FID, or taking the initial value of the FID. For simple materials with only a single proton environment, these methods usually agree to within 0.1 %. For complex materials, which may have several proton environments, integrating spectral peaks can differentiate relaxation times between species, and we use this method because of its proven and common use.

If the local fields at each spin packet are time dependent or the spins diffuse/flow to neighboring spin packets, then the observed T_2 will depend on the value of τ_{cp} . Phase differences due to field variations on time scales slower than τ_{cp} will be rephased, while differences due to field variations faster than τ_{cp} will not be rephased. *Here, we will define T_2 as the transverse relaxation time when measured with a particular value of τ_{cp} .* For our base measurements, we use $\tau_{cp} = 1.0$ ms. The measurement protocol includes the measurement at two values of spin echo times, $\tau_{cp} = 1.0$ ms and $\tau_{cp} = 10$ ms, to identify the presence of any variation of T_2 with refocusing time.

3.3. Model Errors

In complex materials, multiple environments for the water proton may not effectively average over the course of a measurement. Hence, there may be several different T_1 and T_2 relaxation times, giving rise to non-monoexponential decay of the signals. We test for this situation by performing a lack-of-fit test, as described in Appendix 1, to verify the hypothesis that the assumed model is reasonable [10]. We further examine the residuals to see if they are randomly dispersed. If the p -value from the lack of fit test is greater than the significance level, $\alpha = 0.001$, and if the residuals are randomly dispersed,

⁵ We use the NMR convention that τ_{cp} measures the time between the end of the 90° excitation pulse and the beginning of the 180° refocusing pulse. The interval between the center of the 90° pulse and the center of the 180° pulse is then $\frac{t_{90}}{2} + \tau_{cp} + \frac{t_{180}}{2}$, whereas the time between the 180° refocusing pulses is $2\tau_{cp} + t_{180}$. Often, in MRI pulse sequences, where the RF pulse durations are much longer, the convention is to make these two quantities to differ by an exact factor of 2.

we accept the data. If these two conditions are not met, we will reject the data set as not being describable by a simple exponential model. The lack-of-fit test can be problematic for high quality data that has little noise because the sum-of-squares due to pure error (SSPE) term in the denominator in Eq. (A1.2) can be very small, which can lead to a small p -value even though the model is accurate. Hence, we examine cases that have p -value $< \alpha$, including a detailed analysis of the residuals, before rejecting data sets.

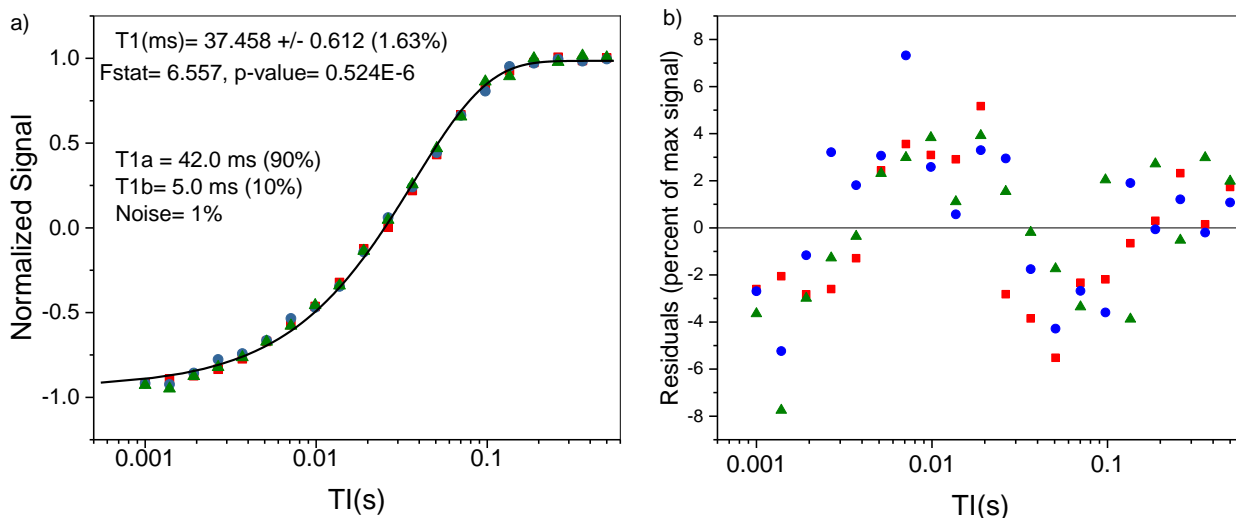


Fig. 1. (a) Synthesized data from an inversion recovery experiment that measures signal proportional to M_z as a function of inversion time TI . These data are biexponential, with 90 % $T_1 = 42.0$ ms and 10 % $T_1 = 5.0$ ms. A Gaussian noise term is also added and the data is repeated three times, similar to the experimental protocol described in Sec. 5.4. (b) Residuals showing structure indicative that the model is not appropriate. The p -value = 0.524×10^{-6} is much less than the significance level of 0.001.

Results from these data would not be reported due to significant lack of fit.

Fig. 1 shows synthesized data obeying Eq. (8) that is similar to what is typically analyzed to obtain T_1 . The data are the result of a bi-exponential decay with relation times of 42.0 ms (90 %) and 5.0 ms (10 %). The fit, using Eq. (8), gives an effective T_1 relaxation time of 37.46 ms. We reject these data because the lack-of-fit test yields p -value = 0.524×10^{-6} , which is much less than 0.001, and the residual distribution is not randomly dispersed about zero.

4. Measurement System

The measurement system, shown in Fig. 2, for proton spin relaxation times consists of a superconducting magnet, an NMR probe with receive/transmit coil tuned to the appropriate ^1H frequency, an RF amplifier, a control box that both generates and records RF signals, a fiber optic thermometer placed next to the sample, and gas flow system and heater to control sample temperature.

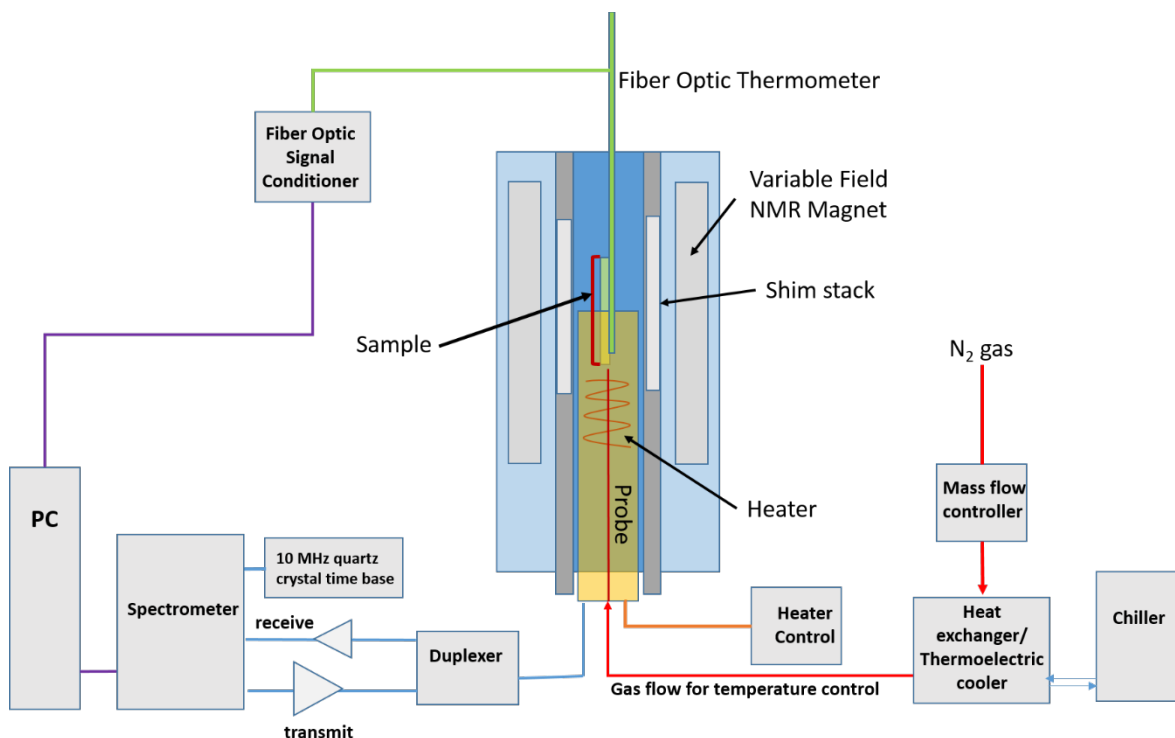


Fig. 2. Schematic diagram of the NIST NMR measurement system.

4.1 NMR system

The NMR system, shown in Fig. 2, was assembled by NIST using commercially-available parts. The NMR magnet is Oxford 300-44 project No: 62440; Magnet No: 93894; Cryostat No: DLN0495/30/1. The NMR spectrometer is Tecmag Redstone HF-1 paired with Tecmag TNMR version 3.3.9 software. The NMR probe is Doty DSI-1425, a triaxial gradient probe with low- and high-frequency RF channels for detection of ^2H and ^1H NMR signals, respectively. The probe is designed to work at frequencies from 42 to 300 MHz corresponding to field strengths of 1 to 7 T. Different tuning wands must be inserted at different operation field strengths, as specified in the manufacturer's instructions. The RF coil is a multi-turn linearly polarized transmit/receive saddle coil with a 14 mm homogenous RF length. The RF coil at maximum power can perform a $\pi/2$ pulse in 8 μs . The probe is set up to take standard 5 mm NMR sample tubes. The gradient coils are water cooled, and there is a gas flow/heater system to control the sample temperature. The main solenoid field and superconducting shims are ramped using a Cryomagnetics 4G-100/SHIM superconducting magnet power system.

Magnetic Field Ramp and Shimming

The magnet is ramped by insertion of a set of down leads and energized using a superconducting magnet power supply following the manufacturer's operation manual for field ramp rates and energizing procedures. Because the magnet is operated at MRI field values, not at typical NMR field values, the magnet manufacturer does not specify field parameters at all the operation fields. The superconducting shim coils are de-energized during the field ramp by opening all the persistent current switches. Field stability is improved by overshooting the target field value by 2 % and then

returning to the desired set point. The resonance of a test sample is measured as the field approaches the desired value in order to monitor the field magnitude, the field inhomogeneity, and the field stability. The field is stabilized within 100 ppm of the target value. The noise spectrum is monitored to ensure that the sample resonance at the final field value is not close to any noise sources or system resonances.

The magnet is shimmed by ramping the nine superconducting shim coil currents (Z, Z2, Z4, X, Y, ZX, ZY, X^2-Y^2 , 2XY) to predetermined values for each field strength. Then an automated shimming routine, the Berger-Braun shimming method, is run to adjust the 19 values of the room-temperature shim currents. The 19 room temperature shims are Z1, Z2, Z3, Z4, Z5, X, Y, XZ, YZ, XY, X^2-Y^2 , Z^2X , Z^2Y , ZXY, $Z(X^2-Y^2)$, X^3 , Y^3 . The values of the room temperature shims are then used to readjust the superconducting shims to minimize the currents in the room-temperature shim coils. Both the peak width and symmetry of the line width are assessed. The line width is required to be less than 1 Hz and the asymmetry, as determined by a Lorentzian fit, is required to be less than 2 %.

The field stability of the system is determined by setting up a 15 hr scan that monitors the resonance peak every 10 min. The magnetic field drift should be less than 2 Hz/hr or 50×10^{-9} /hr (50 ppb/hr).

NMR time base verification:

To verify the accuracy of the NMR console oven-controlled crystal oscillator (the system time base that has a nominal frequency 10 MHz), a frequency counter calibrated against a NIST-traceable rubidium frequency reference is used. The measured frequency of the NMR time-base oscillator is $10.000\ 000\ \text{MHz} \pm 5\ \text{Hz}$.

Probe tuning:

To minimize sample-to-sample variations, the RF probe resonance condition is verified on a vector network analyzer by monitoring the reflection coefficient (also known as S11 measurement). The RF probe resonance, where minimal RF power is reflected during the S11 measurement, is adjusted to the frequency of the NMR with the material under test (MUT) and associated sensors appropriately placed inside the NMR probe. Frequency position of the resonance is controlled by a variable capacitor “Tune”. The resonance is also adjusted by a variable capacitor “Match” to adjust the circuit to 50 ohm which can be identified by maximizing the absorption of RF power in the S11 measurement. After tuning the RF probe, a nutation experiment is carried out for each sample following the procedure described next.

NMR radiofrequency (RF) power calibration:

RF power is calibrated using a nutation procedure that records the signal amplitude as a function of RF pulse width τ_{RF} . The calibration is done using the MUT before each sequence of measurements. The RF pulse amplitude, B_{1amp} , remains fixed. For our NMR system, the RF amplitudes are typically between 400 to 500 μT , which is much larger than chemical shifts or B_0 distortions. Hence, for the reference frame rotating with the applied RF field, the B_1 field is stationary and lies approximately in the transverse plane. The signal amplitude, S , is defined as the integral of the real part of the spectra obtained from the FIDs. An example of a nutation data set is shown in Fig. 3. For an ideal system, with a constant B_1 amplitude across the sample, we would expect the signal to vary as $S(\tau_{RF}) = S_0 \sin(\gamma B_1 \tau_{RF})$. However, measured samples are in long capillaries (see Sec. 5.2) that extend beyond the saddle coil in the z -direction, so the RF field is necessarily inhomogeneous. Fig. 3a shows a model

fit to the nutation curve assuming a trapezoidal RF field profile shown in Fig. 3b. The model predicts a signal given by: $S(\tau_{RF}) = S_0 \int \sin(\gamma B_1(z)\tau_{RF}) B_1(z)/B_{1amp} dz$ where the integral is over the RF coil z-axis and the coil sensitivity function, proportional to $B_1(z)$, is included. The first maximum found by this method is noted as the 90° RF pulse; all other flip angles are calculated as a linear extrapolation of time. The variation in B_1 must be considered in the error analysis. For samples with length less than 10 mm, the B_1 variation is much smaller if the sample is well centered. The nutation curve is considerable less damped, and a more accurate model of the RF profile is required to fit the nutation curve.

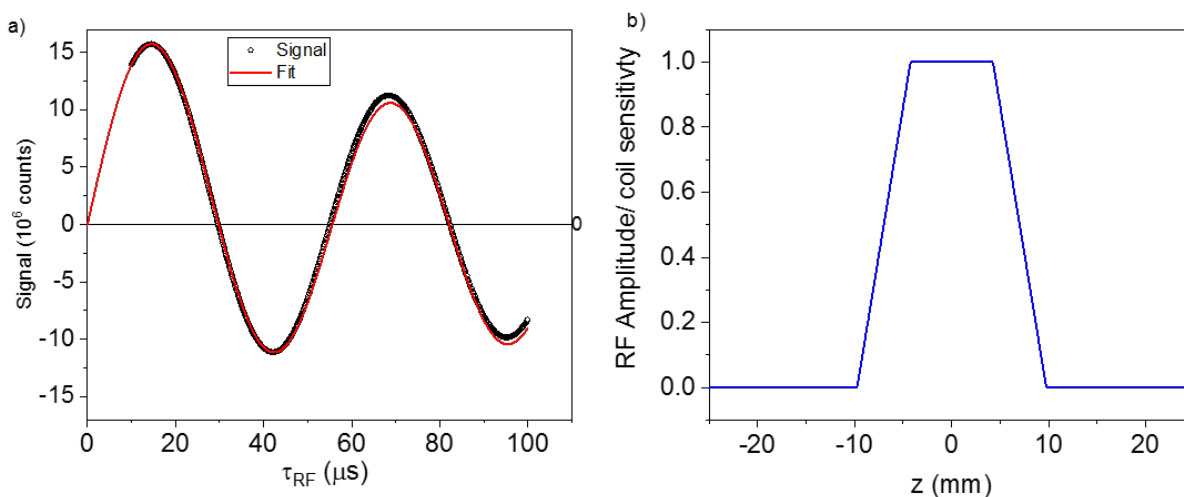


Fig. 3. (a) Nutation data for a MnCl_2 solution (T2-9) at 20°C . The sample length is ~ 50 mm and therefore extends well beyond the RF homogenous region. Red line is a fit using a model where the RF amplitude and coil sensitivity function are given by the graph in (b).

NMR instrument linewidth:

After equilibration, a single spectrum of American Chemical Society (ACS) reagent-grade water is acquired with eight free-induction decay measurements averaged together. The spectrum is then Fourier transformed and processed to provide a vertically positive peak as observed by the NMR operator. The line is then fit with a Lorentz model to determine the FWHM of the single water peak. From this procedure, the minimum linewidth of the instrument was determined to be 0.9 Hz under the conditions used for measurement service experiments.

4.2 Fiber optic temperature probe and temperature control system

The non-magnetic fiber optic probe used to monitor and control the NMR sample temperature is checked against a water triple point cell (273.16 K) and a gallium melting point cell (302.9146 K, per NIST 260-157) once per year. The fiber optic sensor is routinely checked against two NIST-traceable platinum resistance thermometers in an ice-water bath at 273 K and in ambient room air at approximately 293 K. If a systematic offset is found in the sensor, it is corrected throughout the experiments and noted in the report.

The fiber optic temperature probe is placed within the NMR tube as shown in Fig. 5. The NMR tube with the sample and fiber optic probe are lowered into the NMR bore and the spindle is allowed to

rest on top of the NMR probe. The temperature is controlled by a proportional-integral-derivative (PID) control system that adjusts the heater current and gas flow, see Fig. 2, to maintain the sample temperature as determined by the fiber optic probe. A screen shot of the measured sample temperature during a typical sample run is shown in Fig. 4. The maximum temperature deviation for this run was 50 mK.

Temperature scans are taken from low to high temperature, with the shimming recommended at each temperature. Measurements begin at low temperatures to minimize effects due to evaporation and distillation.

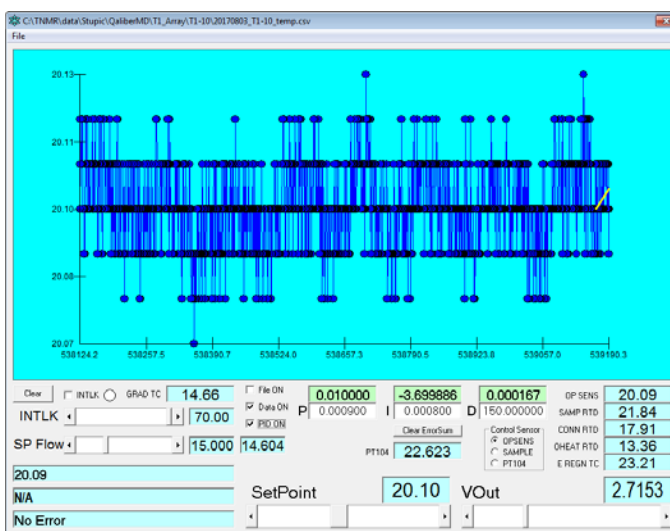


Fig. 4. Screen shot of sample temperature control software with the temperature monitored for 20 min.

5. Standard Operating Procedures

5.1 System Startup

All electronics and other support systems are powered on at least 24 h prior to the start of a measurement. All test equipment is allowed to equilibrate with room temperature. The superconducting magnet and superconducting shims are allowed to stabilize for at least 24 h after ramping currents. Stabilization is particularly important for the quartz crystal oscillator time base and RF amplifier.

5.2 NMR Sample Preparation

The preferred sample configuration consists of 20 μ l aliquots of each material sealed into 2 mm outside diameter (OD) borosilicate glass or 3 mm OD polytetrafluoroethylene (PTFE) NMR tubes. Borosilicate glass samples are flame-sealed with a butane torch. PTFE samples are sealed with a PTFE plug inserted 1 cm into the sample tube. The sample tube lengths are \sim 70 mm, while the filled volume is \sim 10 mm in length. Samples with filled volumes that extend beyond 10 mm can also be measured; however, there will be additional calculable error since the sample will extend beyond the uniform region of the RF coil. Sealed aliquots are inserted into standard 5 mm OD NMR tubes, as

shown in Fig. 5. The insertion depth of the NMR tube was adjusted so that the center of the RF coil is 7 mm above the base of the NMR tube. The fiber optic temperature probe is positioned in the NMR tube so that the sensor will lie 22 mm above the bottom of the NMR tube, 15 mm above the center of the measurement zone. Each sample is equilibrated at the desired temperature for a minimum of 15 min before measuring. The sample bobbin is weighted to prevent the nitrogen flow from lifting it. The samples are stationary during these measurements, since the presence of the fiber optic thermometer precludes spinning. Samples are shimmed using the Berger-Braun shimming method prior to collecting relaxation time data [2].

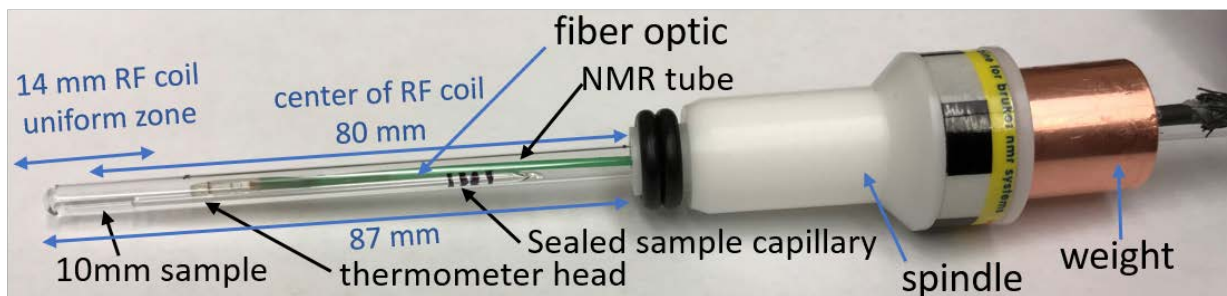


Fig. 5. Sample capillary and fiber optic thermometer inserted into NMR tube, which is then inserted into a plastic spindle before insertion into the bore of the NMR spectrometer.

5.3 Data Acquisition

Inversion recovery (IR) for T_1 measurement:

NMR-IR experiments are conducted by monitoring the longitudinal relaxation of ^1H nuclei at a frequency corresponding to 64 MHz, 128 MHz or 300 MHz (± 20 kHz) using a composite 180° RF inversion pulse. The composite pulse consists of a 90° pulse on $\pm y'$, a 180° pulse on $\pm x'$, and a 90° pulse on $\pm y'$. The composite pulse reduces errors due to inhomogeneous RF fields and provides a more uniform tip angle [11]. Each reported T_1 value is a collection of 20 inversion time (TI) spectra. Each inversion time spectrum is the averaged accumulation of eight phase-cycled free-induction decay measurements listed in Table 1. The composite inversion pulse, the detection pulse, and the receiver phases are cycled. The receiver phase mirrors the phase of the 90° detection pulse so that the detected FID signal is a maximum at the start of the FID. The delay between measurements, TD , is required to be greater than five times the T_1 value [2].

Table 1. Phase cycling scheme showing the eight measurements that are averaged to get the FID that is analyzed to obtain a signal proportional to the longitudinal magnetization. The first three columns are the three components of the 180° composite pulse.

RF Composite 180°			RF Detection	Receiver
90°	180°	90°	90°	
y'	x'	y'	x'	x'
$-y'$	$-x'$	$-y'$	x'	x'

y'	x'	y'	$-x'$	$-x'$
$-y'$	$-x'$	$-y'$	$-x'$	$-x'$
y'	x'	y'	y'	y'
$-y'$	$-x'$	$-y'$	y'	y'
y'	x'	y'	$-y'$	$-y'$
$-y'$	$-x'$	$-y'$	$-y'$	$-y'$

Carr-Purcell-Meiboom-Gill (CPMG) for T_2 measurement:

NMR-CPMG experiments are conducted by monitoring transverse relaxation of ^1H nuclei at a frequency corresponding to 64, 128, 300 MHz (± 1 MHz). The NMR experiment consists of a 90° RF pulse to align spins in the transverse plane and then a train of n hard 180° RF refocusing pulses with a delay of τ_{cp} before and after the refocusing pulse (τ_{cp} is nominally 1.0 ms in length) [12]. Each reported T_2 value is derived from a collection of 20 spectra varying the CPMG acquisition time $t_a(n) = n(2\tau_{cp} + t_{180})$, which is the length of time between the completion of the 90° excitation pulse and the start of the data acquisition. Each CPMG time spectrum is the averaged accumulation of eight free-induction decay measurements. The delay between measurements is required to be greater than five times the T_1 value, as determined by NMR-IR measurements. Other measurement conditions recorded include NMR field strength, NMR time base verification, NMR RF power calibration, NMR instrument linewidth, sample temperature, sample formulation or sample ID number, and NIST ID number.

5.4 Data Analysis

Inversion recovery (IR) for T_1 measurement:

Free-induction decay spectra are Fourier transformed and processed such that the first inversion time spectrum results in an inverted signal. The same processing is applied to all remaining spectra such that signals go from most negative to the most positive as a function of inversion time (see Fig. 6). A phase adjustment is done with the same phase shift applied to all of the data to ensure that the real parts of the Fourier transforms are symmetric and do not change sign. Peak integration is calculated using a trapezoidal rule with integration limits ± 10 times the peak width at 50 % of the peak value. Peak integral values from each inversion time spectrum are fit with an exponential function of the form described in Eq. (5), as shown in Fig. 6. An unweighted, nonlinear least-squares fitting algorithm is used to obtain parameter estimates. \mathbf{A} is a fit parameter that corresponds to the maximum signal at long times. \mathbf{B} is a fit parameter that indicates the degree of inversion obtained with the initial 180° pulse and has a value of 2 for complete inversion of the spins. Initial guess values are taken as $\mathbf{A} =$ the signal of the maximum TI , $\mathbf{B} = 2$, $T_1 = TI$ for the minimum of the absolute values of the data divided by $\log(2)$. These initial values are usually within 10 % of the final fitted values. We require that the \mathbf{B} parameters be between 1.97 and 2.00 for samples of length 10 mm or less or be between 1.90 and 2.00 for samples of length $\gg 10$ mm. The sample position, RF power, and probe tune are adjusted to insure a suitable level of inversion. Typical standard errors from the estimated covariance matrix for the nonlinear least squares fit for all parameters are < 0.1 %. For the sample shown in Fig. 6, fitted T_1 times for the three measurements were averaged, resulting in $T_1 = 42.558 \pm 0.0054$ ms,

where 0.0054 is the standard deviation of the three T_1 values. The coefficient of variation (standard deviation over the mean) is $\text{CoV} = 1.3 \times 10^{-4}$. Simultaneous fitting of all three data sets together gave a similar value, $T_1 = 42.558 \pm 0.012$ ms, where 0.012 is now the standard error in the fit. The lack-of-fit test yields $p\text{-value} = 0.9998$ and the residuals are randomly dispersed, indicating that the model used is appropriate. The standard deviations and standard errors listed above are included in the total uncertainty calculations detailed in Sec. 7.

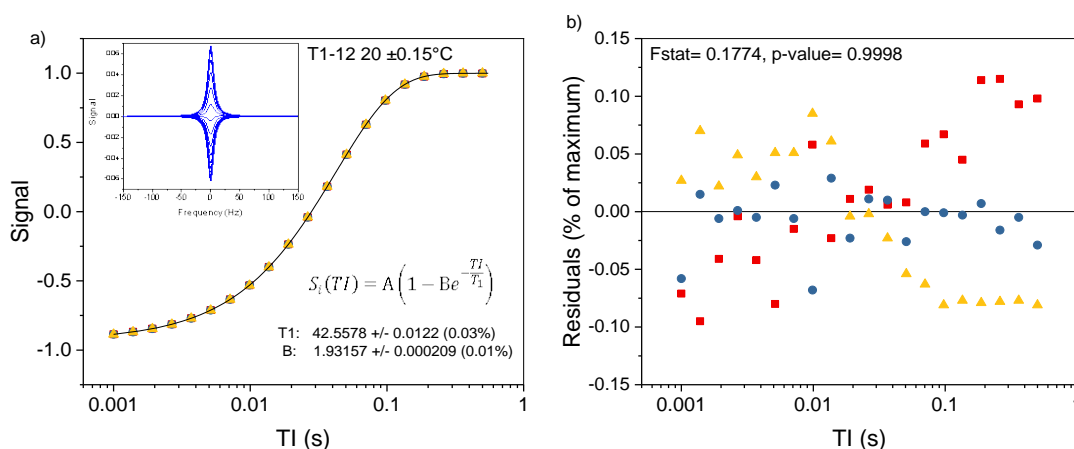


Fig. 6. Inversion recovery data for a NiCl_2 solution which had a filled length of ~ 50 mm: (a) Area of the real part of spectra plotted as a function of the inversion time TI . The data show results from three identical runs. The solid line is the fit to Eq. (8) used to obtain T_1 . The inset shows the real part of spectral data used to generate the integrated signal vs. TI plot. (b) Residuals from the three inversion recovery sequences.

Carr-Purcell-Meiboom-Gill (CPMG) for T_2 measurement:

Free-induction decay data are Fourier transformed and then a phase shift is applied to compensate for the unknown receiver phase delays. The phase shift is determined by making the real part of the spectra positive definite and symmetric and the imaginary part antisymmetric. The same phase shift is applied to all spectra. Typically, the last two CPMG experiments, with the longest acquisition times, should be close to the noise floor to ensure a full data set for T_2 measurements. The real part of the spectra, shown in the inset in Fig. 7a, are integrated using the trapezoidal rule. The peak integration interval for the spectra is set to be ± 10 FWHM around the peak center, where FWHM is the full-width at half-maximum of the first spectrum. Peak integral values are plotted (Fig. 7) as a function of acquisition time $t_a(n) = n(2\tau_{cp} + t_{180})$, where t_a is the time duration between the initial excitation and the start of data acquisition, n is the number of 180° inversion cycles, τ_{cp} is the length of the delay before and after the 180° pulse (including all transmit/receive blanking/activation delays), and t_{180} is the duration of the 180 RF pulse. Peak integral values from each CPMG time spectrum were fit with an exponential function in Eq. (10).

For the sample in Fig. 7a, fitted T_2 times were averaged together giving $T_2 = 30.587 \pm 0.011$ ms. Further, all data were analyzed together giving the same T_2 value to within $1 \mu\text{s}$. Fig. 7a shows two fits, one for the complete data set (black line), the other for the first 14 data points that are well above the noise floor (blue line). The extracted T_2 values are the same to within $1 \mu\text{s}$, indicating little variation with the range of the fit. The residuals are shown in Fig. 7b, and the p -value from the lack-

of-fit test is 0.0045. There is a small deviation in the uniformity of the residuals at small times, indicating the possible presence of a short relaxation time component. However, the values of the residuals are very small, indicating that a second component, if present, constitutes less than 0.1 % of the signal. The total uncertainty in T_2 is calculated using a comprehensive method discussed in Sec. 7.

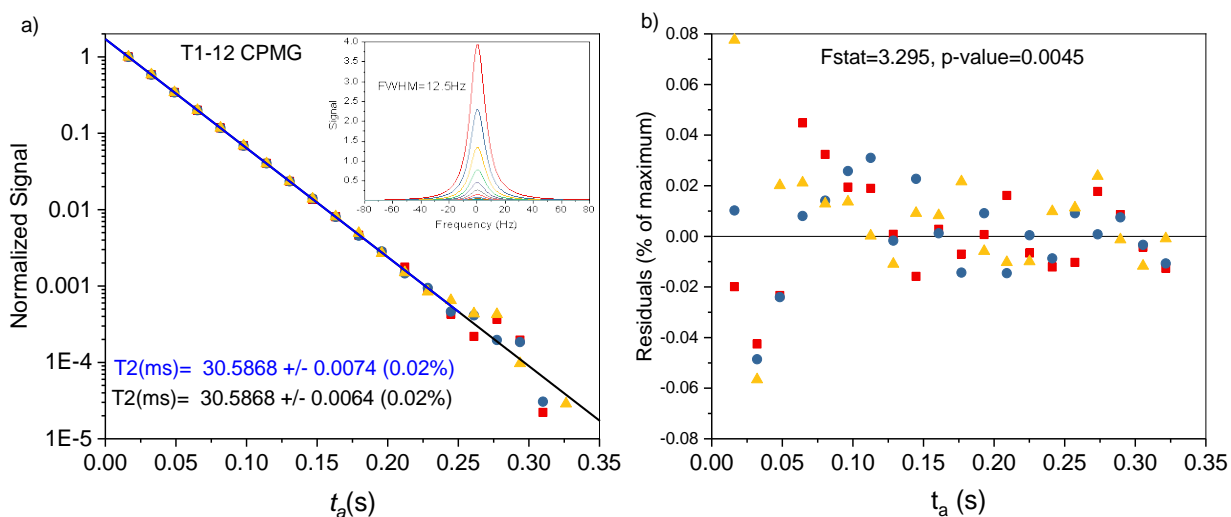


Fig. 7. T_2 measurement of same sample as used in Fig. 6. (a) Area of the real part of the spectra as a function of $t_a = n(2\tau_{cp} + t_{180})$ in a CPMG sequence, which is repeated 3 times (repeats are distinguished using circle, square, and triangle symbols). The solid lines are the fits to all 60 data points to Eq. (10) using only the first 14 shortest t_a times (blue) and using all 20 t_a times (black), illustrating the robustness of the derived T_2 value regarding the region selected for fitting. The inset shows the spectra from which the data are derived. The spectra are fit with a Lorentzian to give a FWHM linewidth of 12.5 Hz, which is used to obtain the inhomogeneous line broadening of 6.4 Hz. b) Residuals showing a small deviation from the model at low acquisition times.

6. Uncertainty Evaluation

Uncertainty is a nonnegative parameter characterizing the dispersion of the measurand [1], in this case T_1 or T_2 . In addition to uncertainty, there will be bias in the measurement. Bias is an estimate of systematic measurement error; it is the difference between the average (expected value) of measurements made on the same object and its true value [1]. The goal of the measurement service is to reduce the bias, through careful measurement and SI-traceability, so that the true value will lie within the uncertainty limits.

The individual uncertainty components for the NIST NMR measurements are estimated following guidelines given in NIST Technical Note 1297 [13]. The uncertainty components are separated into Type A uncertainty evaluations, obtained statistically from a series of measurements, and Type B uncertainty evaluations, determined by subjective judgment or other non-statistical methods.

For Type A uncertainty evaluations, we assume that measurements are independent and normally distributed. For example, the standard uncertainty, $u_{Type A}$, associated with a single measurement of a component (assuming there are no other sources of uncertainty associated with the component) is

$$u_{Type A} = \sqrt{\frac{1}{N-1} \sum_{h=1}^N (x_h - \bar{x})^2}, \quad (13)$$

where x_h represents the individual measurements of a value, \bar{x} is the average of the measurements, and N is the number of measurements made.

For Type B uncertainty evaluations, we typically assume that the value of a component is uniformly distributed. For example, the standard uncertainty, $u_{Type B}$, for a single value of a component (assuming there are no other sources of uncertainty associated with the component) is

$$u_{Type B} = \frac{\delta}{\sqrt{3}}, \quad (14)$$

where the value has an equal probability of being within the region, $\pm\delta$, and zero probability of being outside that region.

Some uncertainty sources arise from both Type A and Type B uncertainty evaluations. For example, the combined standard uncertainty, u_c , for a linear measurement equation is

$$u_c = \sqrt{\sum_{i=1}^{n_A} u_{i, Type A}^2 + \sum_{j=1}^{n_B} u_{j, Type B}^2}, \quad (15)$$

where n_A and n_B represent the number of components associated with Type A and Type B uncertainty evaluations, respectively.

Uncertainties for the measurands T_1 and T_2 are calculated via a Monte Carlo method using the Bloch model. The inputs are worst-case determinations of experimental and calibration uncertainties that go into the measurement process.

6.1. Overview of Measurement System Uncertainties

The sources of uncertainty for the T_1 and T_2 measurements are indicated schematically in Fig. 8 and can be categorized by where they occur in the measurement chain and whether they are type A or B. The traceable calibrations (TC) include calibration of the system time base and the sample temperature probe. The major source of uncertainty comes from non-idealities of the pulse sequences (NPS) due to hardware limitations and to local environment (LE) factors that cause non-uniformities in B_0 , B_1 , and temperature. There will be uncertainties due to non-ideal material properties (NM) such as lack of stability and lack of Bloch model applicability. While these material uncertainties are described here, they are the responsibility of the customer. Finally, there are uncertainties due to data analysis (DA) methods including procedures such as baseline subtraction, integration range, phasing of the complex signals.

The individual uncertainty components are described below. The total uncertainty is calculated by a Monte Carlo method, described in Sec. 7, in which measured or *worst-case distributions* of the relevant parameters are fed into a Bloch simulator and distributions in relaxation times are calculated. A worst-case distribution is defined for each parameter based on observable properties of the measurement system, data, and a defined tolerance for the uncertainty. For example, the B_0 uncertainty is taken from the measured inhomogeneous linewidth, described in Sec 6.4, and a worst-case distribution is defined as a Gaussian distribution with a standard deviation of $0.125 \mu\text{T}$. *The worst-case distributions are used in the Monte Carlo calculation to generate the total uncertainty reported to the customer.* The measured parameter distributions are used to directly compare the uncertainty in measured data sets with calculated uncertainties to validate the model.

A typical set of uncertainties for T_1 and T_2 measurements are given in Table 2. These uncertainties will be evaluated for each measurement and will vary depending on the condition of the measurement equipment and customer sample properties.

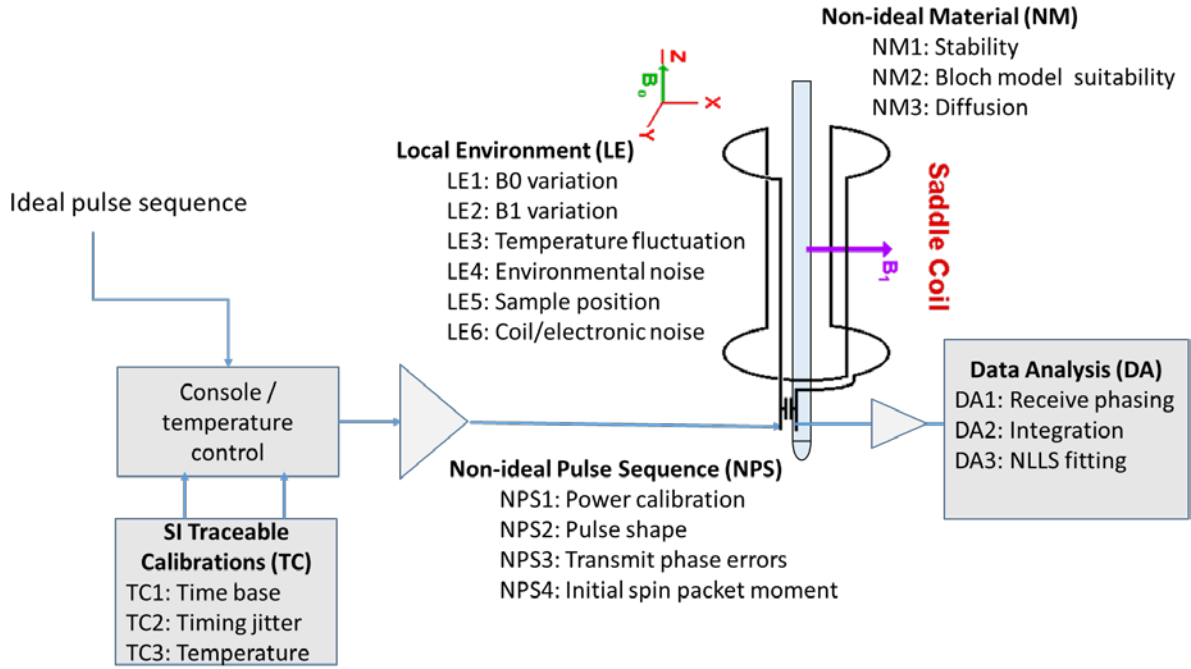


Fig. 8. NMR system schematic with labeled sources of uncertainty

Time base (TC1) and time jitter (TC2)

Proton relaxation times are based on measuring the time dependence of the sample magnetization decay. The measurement of time intervals is based on a complex programmable logic device counting cycles of a 50 MHz frequency reference produced by a 10 MHz temperature-stabilized quartz crystal oscillator. The oscillator is calibrated against a NIST frequency reference to insure errors are less than ± 0.5 ppm and a frequency drift of less than 1 ppm/yr. Other sources of timing errors come from jitter in the NMR time base and digitization in the programmable logic devices controlling the system. The maximum measured jitter in the NMR time base, over the time intervals used in these measurements has a Gaussian distribution with a standard deviation of 60 ps. The uncertainty in a measured time interval Δt is composed of two components, an uncertainty given by the calibration of the time base, U_{tbc} , and a timing jitter U_{tj} :

$$\begin{aligned}
 U_{tbc} &= R * \Delta t * 0.5 * 10^{-6} \\
 U_{tj} &= t_j(60 \text{ ps})
 \end{aligned}
 \tag{16}$$

where R is a continuous uniform distribution from -1 to 1 and t_j is a Gaussian distributed time with a standard deviation of 60 ps. For short times, such as RF pulse durations which are typically 30 μs , the 60 ps jitter dominates the uncertainty. For longer times, such as TI and t_a values, which can be up to 1 s, the uncertainty of the time base dominates. The timing jitter is stochastically varied every timing event, and the calibration uncertainty is stochastically varied after each complete measurement. In general, timing uncertainty contributes less than 100 ns uncertainty in relaxation time values and,

given proper calibration and maintenance of the NMR system, is not a major contributor to the total uncertainty.

The accuracy of the transmit frequency is not relevant for these measurements since the transmit frequency is calibrated using the MUT. However, the transmit phase accuracy and phase stability are critical since variations in the transmit phase will lead to variations in the observed FIDs and hence errors in the relaxation time measurements. The primary transmit phase reference is the phase of the RF field during the spin excitation event. This phase sets the phase of the proton precession. As long as the transmit path and probe tuning do not change during the pulse sequence, subsequent RF pulses will be properly referenced to the initial excitation pulse with the exception of variation due to phase noise. The uncertainty due to phase noise is determined by applying a distribution to the nominal applied transmit phase given from a measured phase noise spectrum.

Temperature calibration/transfer (TC3):

The uncertainty in the sample temperature arises from errors in the sample thermometer calibration and from potential temperature differences between the sample and the nearby sample thermometer. The sample thermometer is calibrated relative to two NIST-calibrated platinum resistance thermometers with errors bounded by ± 0.010 °C. The errors in the sample temperature, T_s , due to miscalibration of the sample thermometer, are bounded by ± 0.150 °C, which corresponds to the maximum drift between calibration intervals. From experiments with changing the thermal coupling between the sample and sample thermometer, e.g., changing the coupling media from air to a high thermal conductivity fluid, the maximum temperature difference is less than ± 0.1 °C. For Monte Carlo simulations, we assume that the temperature uncertainty is given by the sum of two random variables, ΔT_t and ΔT_{cal} , where ΔT_t is uniformly distributed over ± 0.1 °C and ΔT_{cal} is uniformly distributed over an interval of ± 0.15 °C. The uncertainties in T_1 and T_2 are then given by:

$$\Delta T_{1temp} = (\Delta T_t + \Delta T_{cal}) \frac{\partial T_1}{\partial T_s}; \quad \Delta T_{2temp} = (\Delta T_t + \Delta T_{cal}) \frac{\partial T_2}{\partial T_s} \quad (17)$$

Typical values of the change in relaxation time with temperature, for NiCl₂ solutions, are $\frac{1}{T_1} \frac{\partial T_1}{\partial T_s} = 1.3\%/^{\circ}\text{C}$; $\frac{1}{T_2} \frac{\partial T_2}{\partial T_s} = 1.3\%/^{\circ}\text{C}$. However, these coefficients vary considerably with field and temperature, as well as with the type of material being tested. While we have chosen to use worst-case uniform distributions of temperature uncertainty, more realistic distributions can easily be substituted in the simulations because they are experimentally determined. Uncertainty in sample temperature is a major source of uncertainty in the measured relaxation times.

6.2 Non-Ideal Pulse Sequence (NPS)

RF power calibration (NPS1):

The RF field amplitude is calibrated by a nutation experiment described in Sec. 4.1. The maximum error/bias in the RF field amplitude is determined from the fit to be $\pm 5\%$. This is taken into account

in the uncertainty calculation by applying a Gaussian distribution of RF power amplitudes with a worst-case standard deviation of 5 %.

RF pulse shape (NPS2):

The RF pulse shapes used for these measurements are all rectangular. There was no significant change in the pulse shape when monitoring the RF transmit pulses except for timing jitter, which is accounted for in TC2.

RF transmit phase error (NPS3):

The RF transmit phase is self-referenced so the phase difference of the main clock to the transmit signal is not relevant. However, phase noise will be present and will cause the transmit phase to vary. This is taken into account by including Gaussian phase noise with a standard deviation of 1° , applied to each RF pulse. This is consistent with phase noise values measured by a spectrum analyzer at an offset frequency commensurate with the typical RF pulse duration.

Initial spin packet moment (NPS4):

The initial spin packet magnetization vector may not be given by its thermal equilibrium value due to insufficient wait time or due to noise being picked up and transmitted by the resonant transmit/receive coil. The wait times for all sequences are a minimum of $5T_1$ from excitation to re-excitation, ensuring that the magnetization is within 0.67 % of the equilibrium value. This incomplete recovery time is taken into account in the Bloch simulator calculation of uncertainties. Additional fluctuations may arise due to noise, particularly if the transmit gate is open before the excitation. These effects can be included in the uncertainty calculation by adding RF noise during the pre-transmit period.

6.3 Local Environment Variation (LE)

B_0 variation: Nonuniformity of the DC magnetic field (LE1):

The uniformity of the DC magnetic field is accomplished using superconducting and room temperature shims. Maximum inhomogeneous linewidths are on the order of 10 Hz (see Fig. 6). These are included in the uncertainty calculation using a Gaussian B_0 distribution with a standard deviation in the range of 0.125 μT to 0.50 μT depending on the obtainable quality of the shimming for a particular set of samples.

Nonuniformity of the RF field amplitude (LE2):

For a given RF pulse applied to the RF coil with a specified amplitude, frequency, phase, and shape, there will be a distribution of RF field amplitudes experienced by the sample determined by the RF transmit coil design and the sample loading. The RF field amplitude was measured along the z -axis to obtain a B_1 field distribution. Since the same coil is used for both transmit and receive, the variation in the RF transmit field also corresponds to a variation in the receive sensitivity. To determine the uncertainty in the T_1 and T_2 measurements, a piecewise linear approximation to the measured B_1 variation is used. The parameters in the model B_1 variation are determined by nonlinear least squares fit to the nutation data.

Temperature fluctuation (LE3):

The temperature is set by a closed loop system that controls a heater and cooled gas flow system and feeds back on a fiber optic thermometer placed next to the sample. The measured thermal fluctuations of the sample thermometer are $< 0.050^\circ\text{C}$. This amplitude is less than the $\pm 0.15^\circ\text{C}$ absolute calibration/-stability of the thermometer. The measurement uncertainties from temperature fluctuations are included in the errors in the thermometer calibration/stability.

Environmental noise (LE4):

Environmental noise is due to RF radiation or low frequency magnetic field fluctuations coming from the vicinity of the NMR scanner. Care is taken to locate the scanner in a low noise environment and environmental noise is monitored by taking repeated scans with the same sample and configuration. If deviations occur in the integrated signal by more than 0.2 % in the sets of three identical repeat measurements, the measurements are halted, and noise issues are fixed before proceeding. *We, therefore, do not take environmental noise into account in the uncertainty analysis.*

Sample position (LE5):

Slight variations in the sample position and orientation of the capillary and fiber optic thermometer may alter both B_0 and B_1 distortions. To determine the error due to sample positioning, a test/retest protocol is used where the sample is removed from the NMR system, the thermometer insertion is redone, the sample is reinserted and measured. For short samples < 10 mm, the sample is centered within the RF coil to ± 1 mm and verified by monitoring the nutation curve and inversion recovery parameters. The Monte Carlo calculations will vary the sample position by ± 1 mm.

Coil noise/electronics noise (LE6):

Coil noise and electronic noise are measured from the spectrometer during an interval when no signal is present. To determine uncertainty, a Gaussian noise term, similar to the measured noise spectra, is added to the simulated signal before the analysis. Typical signal-to-noise ratio (SNR) values are between 2000 and 20000. A typical worst-case SNR is between 2000 to 5000, depending on the data set. This is then used to determine the Gaussian noise standard deviation, which is given by the maximum observed signal divided by the worst-case SNR.

6.4 Non-ideal material properties (NM)

Stability (NM1):

There are a number of possible causes for this non-ideality. The supplied materials may not be stable and may change properties during shipping, transferring into the measurement capillary, or due to insertion into a high magnetic field environment. The content of dissolved gases, such as oxygen, which can modify proton spin relaxation, can change over time or during sample handling. Samples can also change during the measurement process due to evaporation/distillation or materials plating out on the sides of the storage or measurement vessels. Care is taken to transfer and seal the samples rapidly to prevent evaporation. For higher temperature measurements, care must be taken so that no distillation occurs which would leave a more concentrated solution at the bottom relative to the top of the capillary. The standard operating procedure is to start at low temperatures and work up in temperature to minimize possible distillation. Samples are visually inspected before and after measurement to ensure that the sample looks homogenous. NIST will exercise care both in handling and in selecting the measurement vessels to minimize change of properties. *However, because NIST cannot control or always know the composition and properties of the samples, the uncertainties due to material instability are the responsibility of the customer. Special handling protocols can be established for particular samples as required, including handling in controlled atmospheres.*

Bloch model suitability (NM2):

The materials supplied by the customer may not have well defined spin relaxation times which will manifest as poor fits to the Bloch equation predictions. If this is the case, the materials will be returned without reported relaxation times.

Diffusion (NM3):

Diffusion of water in an inhomogeneous field can lead to additional dephasing of the proton spins. The shim on the NMR insures that the field inhomogeneities are on the order of 10 Hz or 0.250 μ T, which are insufficient to give additional contributions to T_2 . However, some samples may have intrinsic nonlocal fields that can lead to diffusion mediated dephasing. We consider this to be intrinsic to the sample and to be included in the reported T_2 with the reported dephasing time.

6.5 Data Analysis (DA)

Receive phase (DA1):

The NMR system has timing delays during receive amplification and digitization. While quadrature signals can be measured precisely, the absolute phase information is lost during the signal detection process. A phase shift is applied to complex data to compensate for the phase delay that occurs during signal reception and detection. Since the receive and digitization processes are the same for all FIDs, all spectra will have the same phase shift resulting in a similar change in signal for all spectra. Uncertainty occurs due to errors in determining the phase shift to be applied. A maximum error in the phase shift was determined to be $\pm 5^\circ$. We apply a flat distribution of phase shift errors of $\pm 5^\circ$ in the Monte Carlo calculation.

Integration/-baseline (DA2):

The spectra are integrated over a range corresponding to ± 10 FWHM, where FWHM is the full-width at half-maximum of the spectra with the maximum amplitude. There is an uncertainty introduced due to the range of the integration and to the non-zero baseline of the data. The baseline is subtracted before integration by measuring the offset in the last 10 % of the spectra. However, this is imperfect, and the error is simulated in the Monte Carlo calculation by adding a random offset to each data set that has a Gaussian distribution with a width equal to that of the maximum observed distribution in baseline values. This value is typically 5×10^{-5} times the maximum signal.

Nonlinear Least Square (NLLS) fitting (DA3):

The data is fit with standard NLLS fitting algorithms using the Levenberg-Marquardt method, such as implemented in `scipy.optimize`. Different fitting algorithms, e.g., linear fits, have been used to determine that the NLLS fits are not the major component of uncertainty. Two independent software packages are used for data analysis to insure agreement between independent codes. Fitting algorithm uncertainties on T_1 , T_2 were less than 0.1 % and are not considered in the Monte Carlo calculation. Another important source of uncertainty, which occurs during fitting to a model, is the handling of data when they approach the noise floor of the system, particularly in the case for fitting CPMG T_2 data. Here, points with magnitude less than three times the noise floor are excluded from the fit.

7. Monte Carlo Uncertainty Calculation

A Monte Carlo approach is appropriate for computing measurement uncertainty when the measurand cannot be represented using the traditional propagation-of-errors method [14], which is the case for uncertainties in T_1 and T_2 measurements. Here, the uncertainty is calculated using a Monte Carlo technique in which distributions of parameters that contribute to the measurement uncertainty, described in Sec. 6, are input into a standard Bloch-solver that integrates the Bloch equations for each event in the NMR pulse sequence. The performance of the ordinary differential equation solver was checked against two other independent solvers on several standard problems to establish that the errors in the numerical integrations were considerably less than the errors from the instrument and sample uncertainties listed above. Fig. 9 is a diagram of the calculation, which consists of three loops.

The first/inner loop integrates over a large ensemble of spin packets, typically 10^5 , where B_0 and B_1 are determined from a random spin packet position within the sample. The second loop is over the desired pulse sequence parameter list, either TI or t_a , with typically 20 values, and includes uncertainties due to timing jitter, phase noise, and sample position. The output from these calculations are then fed into a data processing pipeline identical to the one used for real data. Additional noise and receive phase errors are added in this stage before a nonlinear least squares fit is done to obtain a T_1 or T_2 value. The third/outer loop then iterates this process with different values of uncertainties to build a distribution of T_1, T_2 uncertainties. These distributions are compared with the model input relaxation times, to determine the measurement bias and uncertainty.

Fig. 10 shows example output from the Monte Carlo calculations when all non-idealities are included. T_1 and T_2 distributions from Monte Carlo calculations are shown, varying all parameters for $N = 100$ trials. The simulation is for a 10 mm long sample of a material that mimics the NIST internal standard Ni-S25. The input T_1 and T_2 values are 44.000 ms and 37.000 ms, respectively. The T_1 distribution shows a statistically significant bias of $58.4 \mu\text{s}$, the deviation of the mean from the true value, and a standard deviation of $97.9 \mu\text{s}$. The derived uncertainty is $294 \mu\text{s}$, defined as $3 \times \text{SD}$, where SD is the standard deviation. The B -parameter in the T_1 inversion recovery fit, which is a measure of B_1 inhomogeneity, had a mean value of 1.993, which is similar to the measured data for 10 mm samples, indicating that the simulation is accurately reproducing system nonidealities. The T_2 distribution shows a smaller bias of $5.0 \mu\text{s}$, which is within the error of the estimate of the mean. The derived T_2 uncertainty is $274 \mu\text{s}$.

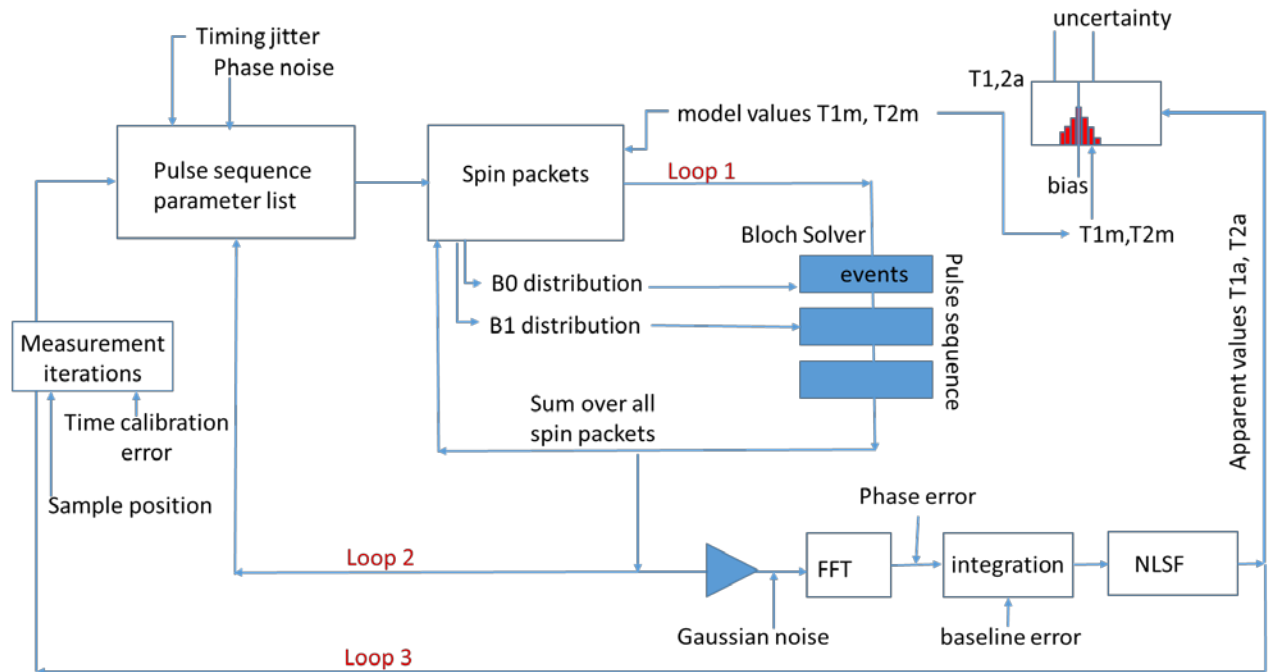


Fig. 9. Schematic of Monte Carlo calculation showing conversion of uncertainties in input parameters into uncertainty in relaxation times.

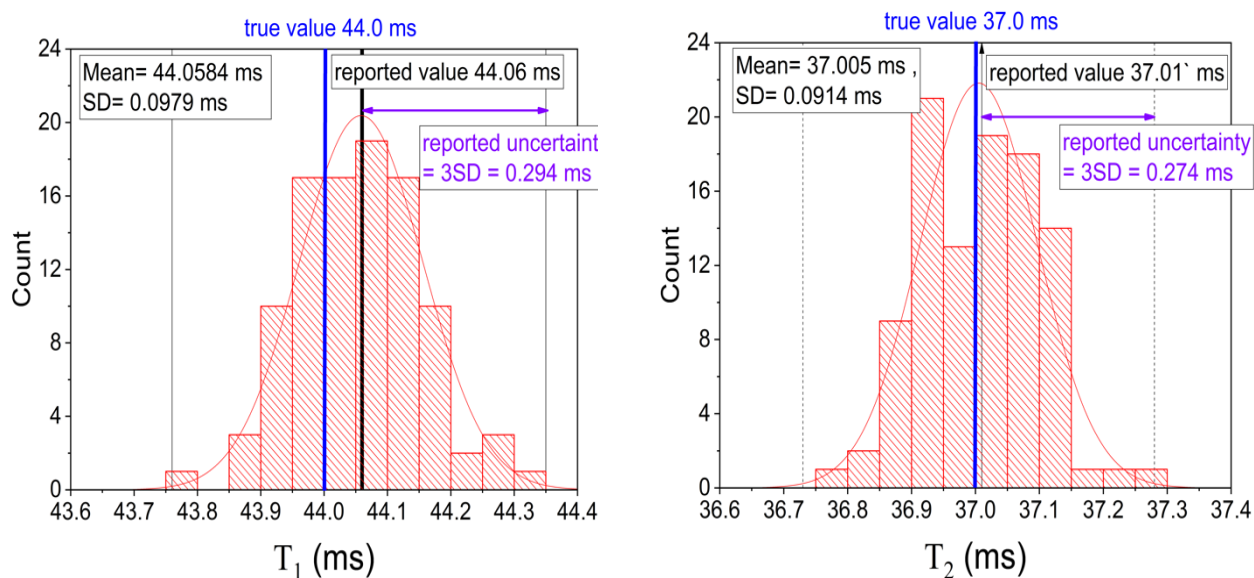


Fig. 10. T_1 and T_2 distributions from Monte Carlo calculations varying all parameters for $N = 100$ trials. The input T_1 and T_2 values are 44.000 ms and 37.000 ms, respectively, which mimics the NIST internal standard Ni-S25.

Table 2 shows the summary output from the Monte Carlo Bloch simulations for the Ni-S25 standard material with a $T_1 = 44.000$ ms, $T_2 = 37.000$ ms. The calculations were done using a Bloch solver using the T1-IR and T2-CPMG protocols and experimental uncertainties described above. The columns labeled T_1 bias, T_1 SD, T_2 bias, and T_2 SD give the bias (mean) and standard deviation of T_1 , T_2 distributions. The table lists simulations where only one given parameter is allowed to vary to indicate which parameters are most important in determining uncertainty. The penultimate row displays the bias and standard deviation when all parameters are allowed to vary, derived from the data shown in Fig. 10. The final row displays the uncertainties in microseconds that would be reported for the experimental measurement of this sample. The total uncertainty simulation was calculated using 100 trials, while the individual uncertainty calculations were done with 40 trials. Each trial mimics an experimental T_1 , T_2 measurement made on different days, with different operators, with the variations in system and environmental conditions that cannot be eliminated. The major sources of uncertainty for this sample are temperature calibrations/transfer/fluctuation, B_1 nonuniformity, and coil/electronic noise.

The reported T_1 , T_2 values are the apparent measured values minus the bias. The reported uncertainty is three times the standard deviation. Therefore, there is > 99.7 % probability that the true value lies within the reported value \pm the uncertainty.

The uncertainty determined using a physics-based Monte Carlo technique is not a simple quadrature addition of the individual uncertainties because different input parameters can interact in complex ways. A distribution in a particular parameter may lead to a small uncertainty in the relaxation times;

Uncertainty Source	Type	Distribution	SD/width	T ₁ bias (μs)	T ₁ SD (μs)	T ₂ bias (μs)	T ₂ SD (μs)
TC1: Time base calibration	B	Uniform	±0.5 ppm	0.0	0.1	0.0	0.0
TC2: Time base jitter	A	Gaussian	σ = 60 ps	0.0	0.0	0.0	0.0
TC3: Temperature calibration	B	Uniform	±0.15 °C				
transfer	B	Uniform	±0.10 °C	1.8	78.5	-11.0	67.8
NPS1: Power calibration, B ₁ amplitude	B	Uniform	±5%	0.0	1.3	0.0	0.0
NPS3: Transmit phase errors	B	Gaussian	σ = 0.05°	0.0	0.0	0.0	0.0
LE1: B ₀ nonuniformity	A	Gaussian	σ = 0.125 μT	0.0	0.0	0.8	5.3
LE2: Quartic B ₁ nonuniformity	A	Uniform	±1.0 mm	14.7	6.3	0.0	0.0
LE3: Temperature fluctuation	A	Gaussian	σ = 0.05 °C	-2.0	14.6	2.1	20.2
LE6: Coil/electronic noise MaxSig /SNR	A	Gaussian	σ = 0.0002	-0.9	9.5	3.4	23.3
DA1: Receiver phase error	B	Uniform	±4°	0.0	0.0	3.8	14.2
DA2: Integration/ base line error	B	Gaussian	σ = 0.00005	0.2	3.1	0.9	4.8
All uncertainties/ nonidealities (μs)				58.4 ± 9.8	97.9	5.0 ± 9.2	91.4
Reported uncertainty (μs)				294		274	

however, when combined with other uncertainties, it may lead to a large contribution to measurement bias and standard deviation. This occurs, for instance, when B₀ and B₁ nonuniformities are combined, where B₀ nonuniformities greatly enhance B₁-induced biases in T₁. The uncertainty will be recalculated if quantities such as temperature dependence, SNR, or sample geometry vary or if there are changes in the measurement apparatus.

Table 2. Results of Monte Carlo calculations of bias (mean) and standard deviation associated with T_1 , T_2 measurements. The calculation was done for a 10 mm long cylindrical NiCl_2 sample, with $T_1 = 44.0$ ms, $T_2 = 37.0$ ms, $dT_1/dT_s = 1.3 \text{ \%}/^\circ\text{C}$, $dT_2/dT_s = 1.3 \text{ \%}/^\circ\text{C}$. The parameters model the NIST internal standard Ni-S25, derived from NIST SRM 3136. The biases and standard deviations below 50 ns are reported as 0.0.

8. Quality Control

NIST's measurement services make use of quality assurance practices to ensure the validity of measurement results and their uncertainties. Such practices include:

- Repeated measurements/calibrations compared over many time intervals;
- Comparison of previous results obtained using multiple measurement methods, if available;
- Routine, periodic measurements with different methods.

For this service, we assess the reproducibility of the NMR measurements prior to each measurement series using Ni standard reference material SRM 3136 diluted to 1 mM, 5 mM, 25 mM Ni^{+2} in high purity 2 % HNO_3 water solutions. The properties of this SRM are detailed in SRM 3136 - Nickel (Ni) Standard Solution Certificate. We calibrate the fiber optic temperature before each measurement series at 0 °C (ice-point) and with traceable platinum resistance thermometers at several temperatures. Additionally, the fiber optic temperature sensor is calibrated with a triple-point water cell and a gallium melt cell every year. The quality control plan for NMR measurements, software version control, and data storage are documented in MRI Biomarker Calibration Service Quality Manual III.

A set of quality control tests are done during data analysis. These include:

1. The recovery times for all experiments are greater than $5T_1$.
2. The lack of fit test yields p -value > 0.001 or the standard deviation of the residuals from the normalized signal is $r_{\max} < 0.001$.
3. The inhomogeneous line width (FWHM) after shimming is less than 10.4 Hz.
4. The **B** parameter in the T_1 inversion recovery fit, which is a measure of RF homogeneity, must be greater than 1.97 for the preferred short sample geometry or greater than 1.90 for the long sample geometry.

If any of these conditions are not satisfied, the problem will be corrected, and the measurement repeated.

Historic data from previous measurements of the NMR apparatus shall be placed into the test folder by the Measurement Services Coordinator after the preparation of the calibration report. The Calibration Leader and the Group Leader shall review the data before signing the calibration reports. If a significant variance from previous results is noted, the Group Leader may require another measurement of the calibration item as a test of measurement system conformance.

9. Summary

NIST provides a measurement service to determine the proton spin relaxation times, T_1 and T_2 , of solutions used in phantoms (calibration artifacts) at a specified field strength and temperature. In this document, we have summarized the basic measurement equations, the measurement procedure, and described the quantities that contribute to the relative standard uncertainty.

References

1. L. G. Kessler *et al.*, The emerging science of quantitative imaging biomarkers terminology and definitions for scientific studies and regulatory submissions. *Statistical methods in medical research*, (2014).
2. S. Berger, S. Braun, *200 and more NMR experiments : a practical course*. (Wiley-VCH, Weinheim, ed. 3rd rev. and expanded, 2004), pp. xv, 838 p.
3. T. C. Farrar, E. D. Becker, *Pulse and Fourier transform NMR; introduction to theory and methods*. (Academic Press, New York,, 1971), pp. xiv, 115 pages.
4. R. L. Vold, R. R. Vold, H. E. Simon, Errors in measurements of transverse relaxation rates. *Journal of Magnetic Resonance (1969)* **11**, 283-298 (1973).
5. A. Abragam, *The principles of nuclear magnetism*. (Clarendon Press, 1983).
6. V. Kuperman, *Magnetic Resonance Imaging: Physical Principles and Applications*. (Elsevier Science, 2000).
7. J. M. Kowalewski , L. *Nuclear Spin Relaxation in Liquids: Theory, Experiments, and Applications*. Series in Chemical Physics (Taylor & Francis, New York, 2006), vol. 2.
8. P. B. Kingsley, Methods of measuring spin-lattice (T1) relaxation times: An annotated bibliography. *Concepts in Magnetic Resonance* **11**, 243-276 (1999).
9. S. Meiboom, D. Gill, Modified Spin-Echo Method for Measuring Nuclear Relaxation Times. *Review of Scientific Instruments* **29**, 688-691 (1958).
10. J. W. Neill, Testing for Lack of Fit in Nonlinear Regression. *Ann. Statist.* **16**, 733-740 (1988).
11. M. H. Levitt, COMPOSITE PULSES. *Prog. Nucl. Magn. Reson. Spectrosc.* **18**, 61-122 (1986).
12. S. Meiboom, D. Gill, Modified Spin-Echo Method for Measuring Nuclear Relaxation Times. *Rev Sci Instrum* **29**, 688-691 (1958).
13. *Guidelines for Evaluating and Expressing the Uncertainty of NIST Measurement Results* (1993).
14. Evaluation of measurement data – Supplement 1 to the "Guide to the expression of uncertainty in measurement" – Propagation of distributions using a Monte Carlo method. *Joint Committee for Guides in Metrology* **101**, (2008).

Appendix A: Lack of Fit Test

An F -statistic is calculated from a ratio of the sum-of-squares due to lack of fit (SSLF) to the sum-of-squares due to pure error (SSPE):

The sums of squares are computed as

$$SSLF = \sum_{i=1}^M \sum_{j=1}^{n_i} (\bar{S}_i - \hat{S}_{ij})^2 \quad (A1.1)$$

$$SSPE = \sum_{i=1}^M \sum_{j=1}^{n_i} (S_{ij} - \bar{S}_i)^2$$

where S_{ij} is the value of the response variable, S , \hat{S}_{ij} is the value of S predicted by the model, and \bar{S}_i is the average response for the i^{th} level of the independent variable, TI or t_a . The j subscript indicates the j^{th} repeat measurement within the i^{th} level of TI .

The F -statistic is calculated as

$$Fstat = \frac{SSLF/(M - d)}{SSPE/(N - M)} \quad (A1.2)$$

Where N = total number of data points, M = number of distinct levels of TI or t_a , d = number of parameters to be estimated ($d=3$ for T_1 IR and $d=2$ for T_2 CPMG). The p -value corresponds to the upper tail of the F distribution: $p\text{-value} = F(F\text{-statistic}, M-p, N-M)$.

If the p -value associated with the test statistic is smaller than the significance level, α , then we reject the null hypothesis and conclude that the assumed model is not reasonable. The significance level is a pre-selected small number and we adopt $\alpha = 0.001$. If the p -value is greater than α , we do not reject the null hypothesis and conclude that there is insufficient evidence to claim that the assumed model is not reasonable. If the p -value is less than α , we reject the model interpretation and will not report relaxation time values with the disclaimer that the data did not sufficiently support interpretation by a simple relation time model.